Journal of Solid State Chemistry 185 (2012) 206–212

Contents lists available at SciVerse ScienceDirect

Journal of Solid State Chemistry

journal homepage: www.elsevier.com/locate/jssc

Structural, energetic and thermodynamic analyses of $Ca(BH_4)_2 \cdot 2NH_3$ from first principles calculations

Peng-Fei Yuan [a], Fei Wang [a], Qiang Sun [a], Yu Jia [a,*], Zheng-Xiao Guo [b,*]

[a] Center for Clean Energy and Quantum Structures, and School of Physics and Engineering, Zhengzhou University, Zhengzhou, Henan 450052, China
[b] Department of Chemistry, University College London, London WCIH 0AJ, UK

ARTICLE INFO

Article history:
Received 30 August 2011
Received in revised form
3 November 2011
Accepted 5 November 2011
Available online 19 November 2011

Keywords:
Inorganic compounds
Ab initio calculations
Band–structure
Thermodynamic properties

ABSTRACT

$Ca(BH_4)_2 \cdot 2NH_3$ is a relatively new compound with potential application in hydrogen storage. Here the fundamental properties of the compound, such as electronic structure, energetic and thermodynamic properties, were comprehensively studied using first-principles calculations. Results from electronic density of states (DOS) and electron localization function (ELF) indicate the covalent bond nature of the N–H bond and the B–H bond. Charge density analyses show weak ionic interactions between the Ca atom and the NH_3 complexes or the $(BH_4)^-$ complexes. The calculated vibration frequencies of B–H and N–H are in good agreement with other theoretical and experimental results. Furthermore, we calculated the reaction enthalpy and reaction Gibbs free energy at a range of temperature 0–700 K. Our results are in good agreement with experimental results in literature. Possible reaction mechanism of the decomposition reaction is proposed.

1. Introduction

Hydrogen storage is an important technological problem in the implementation of fuel cells in the automotive industry [1]. One way of storing hydrogen is to use complex metal hydrides, for example, alanates [2,3], amides [4,5] and borohydrides [6–8]. Among these, borohydrides are good candidates because of their high hydrogen capacity. For the metallic borohydrides studied, $Ca(BH_4)_2$ is a promising one due to its relatively high hydrogen capacity 11.4 wt%. Furthermore, the dehydrogenation enthalpy of the material is calculated to be 32 kJ/(mol H_2) [9], within the optimal range for mobile applications, if the decomposition takes place in the following way:

$$Ca(BH_4)_2 \leftrightarrow 2/3CaH_2 + 1/3CaB_6 + 10/3H_2(9.6\,wt\%H_2), \quad (1)$$

In experiment, the thermal decomposition reaction of $Ca(BH_4)_2$ involves two dehydrogenation steps. The first decomposition step starts around 350 °C and leads to the formation of CaH_2; the second step happens in the temperature range of 390–500 °C where an unknown intermediate phase decomposes [10]. Unfortunately, for on-board vehicular applications, their dehydrogenation temperatures are too high. In practice, hydrogen needs to be extracted using waste heat from proton exchange membrane (PEM) fuel cells. The operating temperature is approximately 80 °C, which is much less than the decomposition temperature of $Ca(BH_4)_2$. Therefore, recent research has concentrated on reducing the temperature of hydrogen release. Following this line of reasoning, amine complexes of $Ca(BH_4)_2$, such as, $Ca(BH_4)_2 \cdot 2NH_3$ [11], were developed for hydrogen storage. $Ca(BH_4)_2 \cdot 2NH_3$ was first mentioned in 1989 [12], but it was investigated as a hydrogen storage material only in 2010 by Chu et al. [11]. This material decomposes under the dynamic flow mode, releasing NH_3. The decomposition reaction can be described as

$$Ca(BH_4)_2 \cdot 2NH_3 \xrightarrow{162\,^\circ C} Ca(BH_4)_2 \cdot NH_3 + NH_3 \xrightarrow{230\,^\circ C} Ca(BH_4)_2 + 2NH_3, \quad (2)$$

However, when this decomposing experiment was performed in a closed vessel (where the maximum allowable hydrogen pressure is 65 bar) hydrogen was directly released, with a boron–nitrogen complex. The dehydrogenation occurs at 190 °C and 5.9 H_2 unit can be evolved upon heating the sample at 250 °C [*note*: for 100 h] giving the material ~11.3 wt% of H. This is due to some of the $Ca(BH_4)_2$ groups breaking down and forming $Ca_3(BN_2)_2$ and BN groups. This can be described as

$$Ca(BH_4)_2 \cdot 2NH_3 \xrightarrow{190\,^\circ C} 1/4Ca(BH_4)_2 + 1/4Ca_3(BN_2)_2 + BN + 6H_2, \quad (3)$$

In order to fully understand the thermodynamics and kinetics of hydrogen release from this material, the systemic studies including both experiment and theoretical calculations are needed. Chu et al. [11] have carried out the experimental study of this material, but there has been no theoretical study on this compound. In this paper, we present a comprehensively theoretical study using first-principles calculations of the properties,

* Corresponding authors.
E-mail addresses: jiayu@zzu.edu.cn (Y. Jia), z.x.guo@ucl.ac.uk (Z.-X. Guo).

0022-4596/$ - see front matter © 2011 Elsevier Inc. All rights reserved.
doi:10.1016/j.jssc.2011.11.009

including structural, electronic, energetic, vibrational and thermodynamic properties of $Ca(BH_4)_2 \cdot 2NH_3$ complex.

2. Computational details

In this work, calculations were carried out within the framework of density functional theory [13] by the projector-augmented wave (PAW) method [14,15] and the generalized gradient approximation (GGA) [16] for the exchange-correlation energy functional, as implemented in the Vienna *ab initio* simulation package (VASP) [17–19]. The GGA calculation was performed with the Perdew–Burke–Ernzerhof (PBE) [20] exchange-correlation potential. $Ca(BH_4)_2 \cdot 2NH_3$ has an orthorhombic structure with space group *Pbcn*. The unit cell contains 76 atoms [11]. The equilibrium lattice parameters were first calculated by a plane-wave cutoff energy of 400 eV and a $5 \times 5 \times 5$ *k*-point mesh in the Monkhorst–Pack [21] scheme. In calculation, self-consistency was achieved with a tolerance in total energy of 0.01 meV, and force on each atom was less than 0.01 eV/Å. The optimized lattice parameter is $a=6.420$, $b=8.339$, $c=12.653$ Å, and the volume of a cell is $V=677.59$ Å^3. This result is in good agreement with the experimental result of Ref. [11], $a=6.4160$ Å, $b=8.3900$ Å, $c=12.7020$ Å and $V=683.75$ Å^3. The subsequent calculations were performed on the optimized structure with the same energy cutoff and a denser $7 \times 7 \times 7$ *k*-point mesh. The electronic properties were analyzed via the electron localization function [22] and the electronic density of states, which were calculated by means of the modified tetrahedron Blochl methods [23].

In order to obtain the reaction free energy, the Gibbs free energies $G=F+PV$ should be calculated. The F is Helmholtz free energy and can be calculated by

$$F(T,V) = E_0(V) + F_{vib}(T,V), \tag{4}$$

where $E_0(V)$ is the total energy (as evaluated in the VASP calculations). $F_{vib}(T,V)$ is the vibration energy, and can be calculated by

$$F_{vib} = \frac{1}{2}\sum_{q,v}\hbar\varpi(q,v) + k_B T\sum_{q,v}\ln[1-\exp(-\hbar\varpi(q,v)/k_B T)], \tag{5}$$

where $\varpi_{v,q}(q,V)$ is the phonon frequency at a fixed volume V and a given q vector, the zero point energy is the vibration energy at $T=0$. The phonon calculations were performed by the frozen phonon method as implemented in the FROPHO [24] code.

In the phonon calculation, the $1 \times 1 \times 1$, $1 \times 1 \times 2$, $2 \times 2 \times 2$ and $5 \times 5 \times 1$supercells with a 0.01 Å small displacement were used for $Ca(BH_4)_2 \cdot 2NH_3$, β-$Ca(BH_4)_2$, $Ca_3(BN_2)_2$ and *h*-BN, respectively. For the Brillouin-zone integration, the $5 \times 5 \times 5$, $5 \times 5 \times 5$, $1 \times 1 \times 1$ and $3 \times 3 \times 3$ grid of Monkhorst–Pack special points were used for these compounds, respectively.

3. Results and discussion

3.1. Structure properties

This compound $Ca(BH_4)_2 \cdot 2NH_3$ is characterized by an orthorhombic structure with the space group *Pbcn*. Each unit cell contains 4 formula units. The structure is shown in Fig. 1(a). Each Ca directly coordinates with four $(BH_4)^-$ groups and two NH_3 groups, forming an octahedron (Fig. 1(b)). Then each $(BH_4)^-$ group is shared by another octahedron to form a quasi 2D network in *ab* plane. So along *c*-axis, this structure can be seen as a layer-like structure (Fig. 1(c)). In the octahedron, Ca atom and four B atoms are in the same plane, the dihedral angle is smaller than 1.5°. The distances N–B are 3.644, 3.941, 3.992 and 3.828 Å, respectively. The distances B–B are 3.924, 4.172, 4.163 and 4.172 Å, respectively. The Ca–N distances are 2.447 and 2.519 Å, and the Ca–B distances are 2.811 and 3.008 Å, respectively. This structure is similar to the octahedral coordination presented in the other Ca-related complex hydrides, e.g. $Ca(NH_2)_2$ [25], CaNH [26], and $Ca(BH_4)_2$ [9,27,28]. The bond lengths of B–H, N–H and distance between Ca–H were also calculated and shown in Table 1, together with the bond angles of H–B–H and H–N–H respectively.

From Table 1, we can see that all the four B–H bond lengths are ~1.23 Å, which are similar to our calculated results in $Ca(BH_4)_2$ (~1.22 Å). The six H–B–H bond angles are in the range of 107.1–111.5°. These unequal bond lengths and bond angles may be caused by the interaction between Ca and $(BH_4)^-$ group. The calculated distances of Ca–H (in $(BH_4)^-$ group) are in the range of 2.361–2.981 Å. For NH_3 complex, the influence of Ca on the structure of the group maybe smaller due to the longer distance between Ca and three H in the group which is 3.088 Å, 3.112 Å and 3.025 Å, respectively. The calculated three N–H bond lengths are ~1.03 Å. The calculated three H–N–H bond angles are 104.8°, 105.5° and 105.5°, respectively. Our calculated results compare well with the optimized findings reported in Ref. [11]. The bond length in the coordinated NH_3 is a litter longer than that of NH_3 in the gas phase (1.020 Å), which is likely due to two main factors: one, the N atom in gas phase NH_3 (Lewis base) donates its lone pair to the Ca cation (Lewis acid). On the other, the presence of dihydrogen bonding between the NH_3 and the adjacent $(BH_4)^-$ may sketch the H–N–H bind in the complex [11]. The calculated shortest distance between H^+ in the NH_3 group and H^- in the $(BH_4)^-$ is 2.011 Å, which is less than the van der Waals distance of the interaction in a dihydrogen bond, 2.4 Å, but longer than in the compound NH_3BH_3, 1.7 Å [29]. This indicated that the dehydrogenation temperature of $Ca(BH_4)_2 \cdot 2NH_3$ may be higher than NH_3BH_3 if the H_2 is produced directly by the interaction between the nearest H^+ and H^-.

3.2. Electronic structure

The calculated energy band of $Ca(BH_4)_2 \cdot 2NH_3$ along the high symmetry lines of Brillouin zone is shown in Fig. 2, where it is clearly seen that the compound exhibits nonmetallic features and the calculated band gap is about 5.6 eV. This band gap is larger than that of $Ca(BH_4)_2$ (~4.9 eV) [9], implying the coordination of the two NH_3 groups enlarging the band gap. In fact, the actual gap could be even larger because of the well-known band-gap underestimate by GGA in semiconductors and insulators. The total and partial density of states (DOS) for $Ca(BH_4)_2 \cdot 2NH_3$ was also calculated and shown in Fig. 3. The total DOS shows three well-separated regions: Region A, below −4 eV (the lower energy region of the valance band); Region B, from −4 to 0 eV (top of the valance band); Region C, above 0 eV (the conduction band). The lowest energy part (from −6.8 to −5.8 eV) of Region A is mainly due to the *s*-states of B and H in the $(BH_4)^-$ group. The NH_3 group has very small contributions to this region. The neighboring area (from −5.8 to −4 eV) is mainly contributed by N *p*-states and H *s*-states in NH_3 group. The total DOS in Region B is mainly attributed to the B *p*-states and the H *s*-states in the $(BH_4)^-$ group, with only small contributions from the N *p*-states. The peaks in the broad conduction band in Region C are mainly originated from the Ca *d*-states; B and N atoms do not contribute much to this conduction band. The above DOS analyses suggest: (i) the covalent bond of N–H is due to the strong *sp* hybridization between them. (ii) the B–H covalent bond is composed of both B-2*s*, B-2*p* and H-1*s* states which form *sp*3 hybrids, similar to those of a CH_4 molecule. The required one electron to form the *sp*3 hybrids is donated by a Ca atom nearby. These bonding

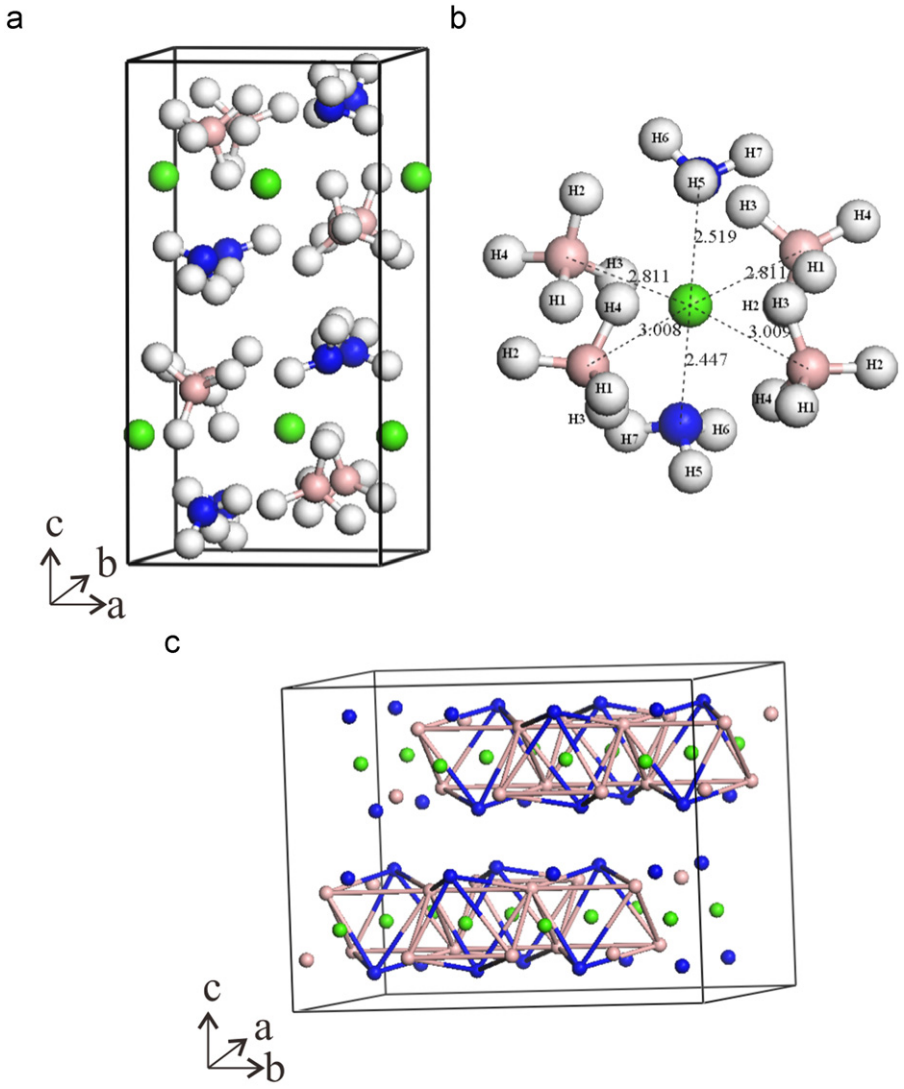

Fig. 1. (a) Crystal structure of $Ca(BH_4)_2 \cdot 2NH_3$. (b) Coordination environment of Ca^{2+}. Each Ca^{2+} coordinates with two NH_3 groups and four $(BH_4)^-$ groups. (c) The layer-like structure along *c*-axis (hydrogen atoms are removed for clearly). Green, pink, blue and white spheres denote Ca, B, N and H atom, respectively. (For interpretation of the references to color in this figure legend, the reader is referred to the web version of this article.)

Table 1
Calculated bond lengths (Å) of B–H, N–H and the distance Ca–H. The calculated bond angles (deg.) of H–B–H and H–N–H are also presented.

Bond length (Å)				
B–H(1,2,3,4)	1.232	1.226	1.231	1.224
N–H(5,6,7)	1.026	1.029	1.030	
Ca–H(1,2,3,4)	2.361	2.981	2.631	2.432
Ca–H(5,6,7)	3.088	3.112	3.025	
Bond angle (deg.)				
H1–B–H(2,3,4)	110.1	109.3	107.1	
H2–B–H(3,4)	109.4	109.6		
H3–B–H4	111.5			
H5–N–H(6,7)	104.8	105.5		
H6–N–H7	105.5			

properties can also be seen in other compounds which include $(BH_4)^-$ ionic group, such as $Zn(BH_4)_2$ [30]. (iii) The interaction between Ca and B atoms or Ca and N atoms is essentially ionic because of no overlapping between their orbitals.

In order to obtain further insight into the chemical bonding of this compound, we have analyzed charge density distribution and electron localization function (ELF). Here, we selected a plane in

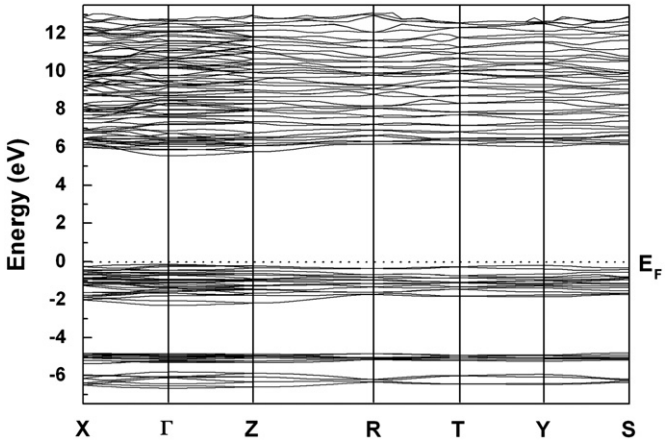

Fig. 2. Calculated band structure of $Ca(BH_4)_2 \cdot 2NH_3$.

which Ca, B and N atoms are all located (Fig. 4(a)). The calculated total valence charge density distribution is shown in Fig. 4(b). The charge density around Ca is considerably high. In $(BH_4)^-$ complexes, the charge density is strongly localized around H atom.

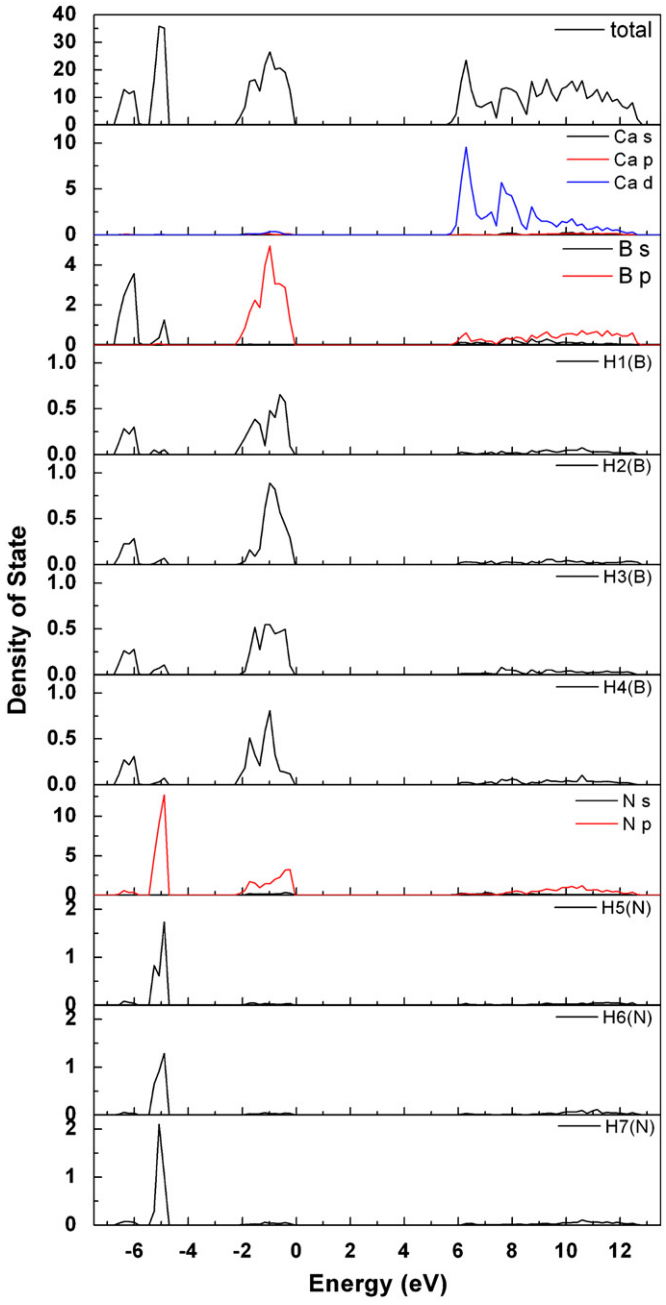

Fig. 3. Calculated total and partial density of states. The Fermi level is set at zero energy.

Almost no charge density is seen around the B atom. This suggests that the electrons are transferred to the H atom mostly from the B atom, resulting in a strong B–H bond in the $(BH_4)^-$ complex with less polar bonding between Ca and H(B) atoms. In the NH_3 complexes, the charge density is localized in the N atom; the density around H is small. There are no overlaps between the Ca atom and the NH_3 complexes or the Ca atom and the $(BH_4)^-$ complexes. This indicates weak ionic interaction between these complexes and the Ca atom. This can be confined by the narrow band widths of the occupied states. In order to visualize the effect of the charge transfer, we also calculated the charge density difference (CDD) between the valence charge density and the superposition of the pseudo atomic charge densities, which is given in Fig. 4(c). For the $(BH_4)^-$ complex, the charge density increases in the H atom, but almost no change around the B atom.

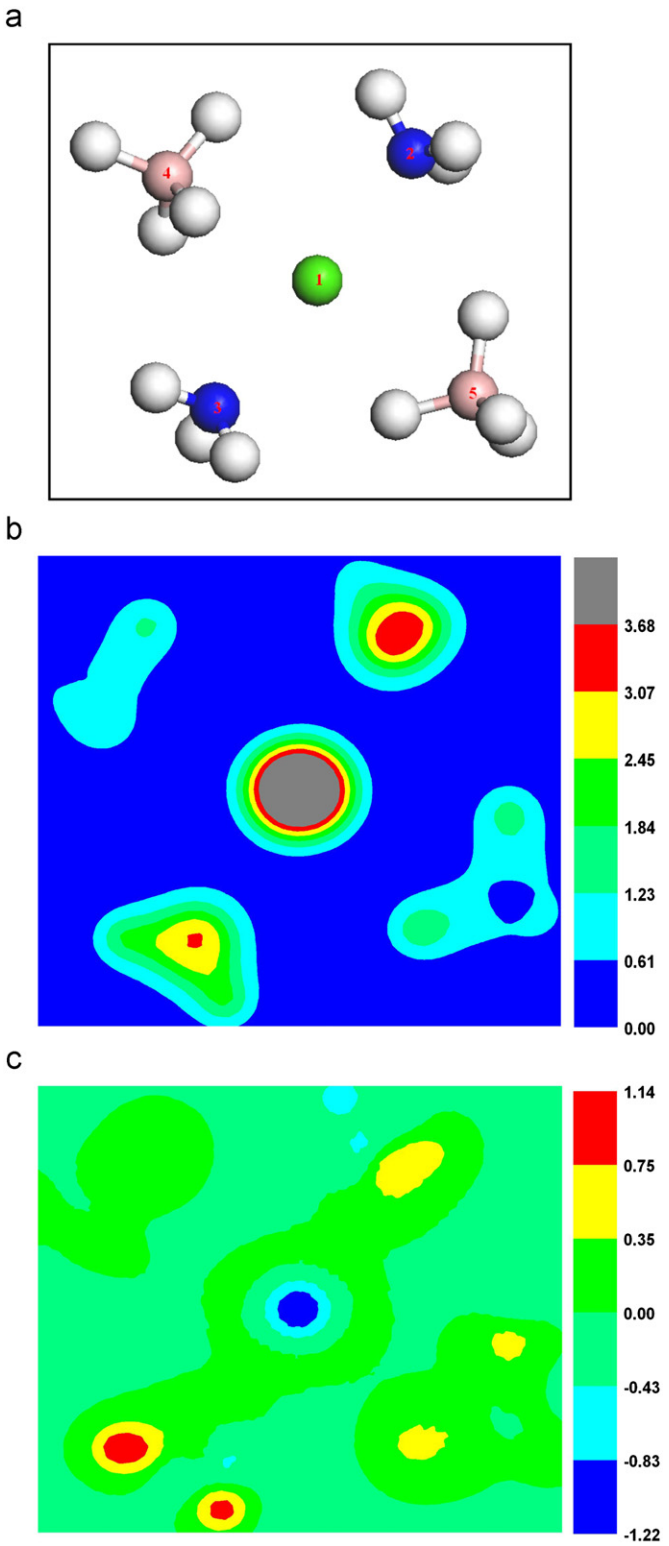

Fig. 4. (a) Atomic position of the selected plane; (b) charge density distribution in the selected plane; and (c) difference in valence-charge density distribution in the selected plane. Green, pink, blue and white spheres denote Ca, B, N and H atom, respectively. (This plane is defined by atom 1, 2 and 5, atom 3 and 4 are not definitely in the plane and the distance is 0.15 and 0.36 Å.) (For interpretation of the references to color in this figure legend, the reader is referred to the web version of this article.)

This is similar to the results in the $Zn(BH_4)_2$ compound [30]. The density around the Ca decreases, and the density around the N increases. In the area between the Ca and the NH_3 complexes the

charge density also increases, but decreases in the area between the Ca and the $(BH_4)^-$ complexes.

The ELF contour plots calculated in two cross-sections parallel to the (010) plane are shown in Fig. 5. The atomic position of the two planes can be seen in the left panel of Fig. 5. ELF is associated with the probability density of finding two electrons in the same spin state close to each other. It is a position-dependent function which varies between 0 and 1. ELF=1 corresponds to perfect localization and ELF=1/2 the electron gas. In Fig. 5(a), the calculated ELF shows strong and large attractors around the H atom. Hydrogen has no core attractor, which indicates either a shared-electron or a closed-shell bond. The very low ELF values around the *B* sites indicate delocalized electrons. A very high value of ELF within the $(BH_4)^-$ complex indicates ionocovalent bonding. In Fig. 5(b), the figure shows a spherical shell attractor around Ca. The ELF value is small between Ca and NH_3 or Ca and $(BH_4)^-$, which indicates weak ionic bond. In the NH_3 complex, the ELF value around the H is also large. The value around N is about 0. And the region between N and H is 0.5. This is characteristic of covalent bond. Furthermore, a finite distribution occurs between the H atoms within the NH_3 complex and the $(BH_4)^-$ complex, which suggests a non-negligible covalent-type of interaction present the hydrogen atoms.

At last, the charges of all the atoms of this compound were obtained by Bader charge analysis [31]. The calculated results are 1.59 e for the Ca atom, 3.0 e for the B atom, −0.95 e for the H atom in the $(BH_4)^-$ groups, −3.0 e for the N atom and 1.0 e for the H atom in the NH_3 groups, respectively. This result indicates that the interaction between Ca and $(BH_4)^-$ groups are totally ionic, and that interaction between Ca and NH_3 groups is a relatively weak ionic interaction, respectively. So the Ca–N interaction may less strong than that of Ca–B even the former is of a shorter distance (2.447 (/2.519) Å vs. 2.811 (3.008) Å). This may be the reason why NH_3 is released during experimental study [11].

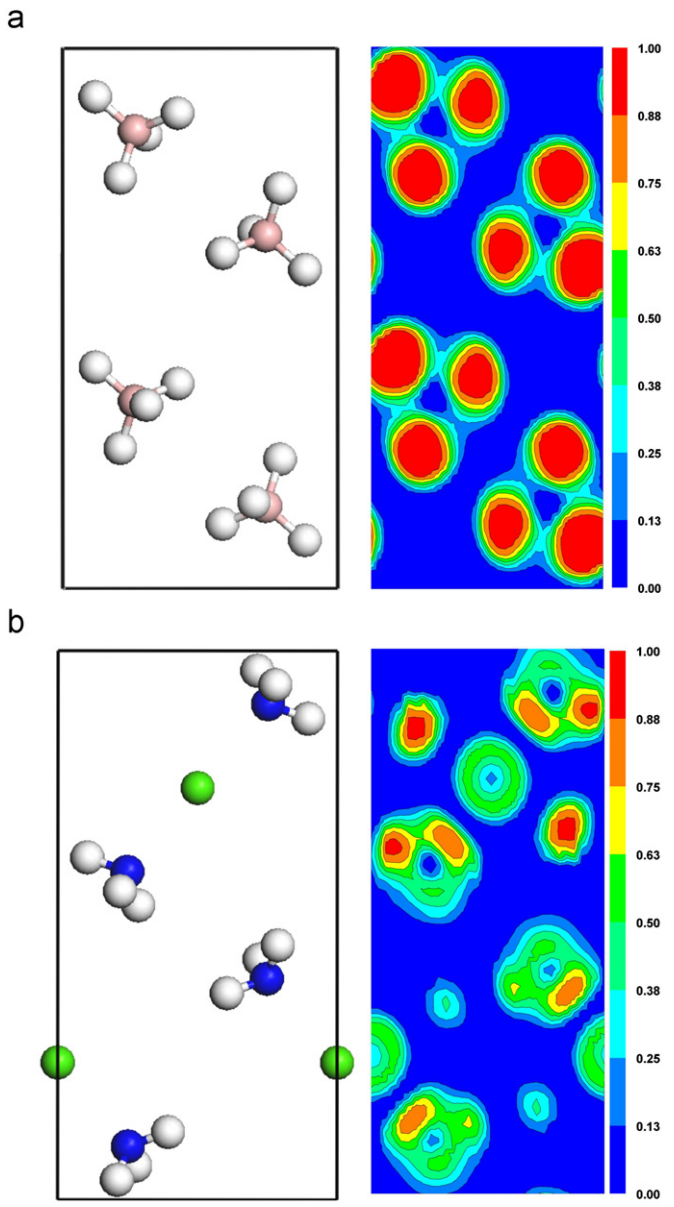

Fig. 5. Atom positions and partial ELF contour plots in (010) plane (a) and (010) plane passing through Ca atom (b). Left panel shows the atom positions and right panel shows the partial ELF contour plots.

3.3. Reaction free energy

In the Section 1 we have already mentioned that there are two different reactions at different conditions: Reaction (2) (release NH_3 under dynamic flow mode) and Reaction (3) (release H_2 in a closed vessel). In this section the reaction enthalpy and reaction Gibbs free energy for the overall Reactions (2) and (3) were calculated. To do so, we need to know the vibrational property of the materials. Here, the calculated phonon spectra of the $Ca(BH_4)_2 \cdot 2NH_3$ within the harmonic approximation are shown in Fig. 6. From the analysis of the eigenvectors, we found the eigenmodes in the regions of 1000–1250 and 2250–2500 cm^{-1}, which originate from the internal B–H bending, and the stretching vibrations in the $(BH_4)^-$ complex anion, respectively. The eigenmodes in the regions of 1500–1700 and 3250–3500 cm^{-1} belong to the internal N–H bending, and the stretching vibrations in the NH_3 complex, respectively. These results compare well with other calculated results for the B–H vibration [30] and the experimental results for B–H [32] and N–H vibrations. We can also see from Fig. 6, the librational frequencies (< 500 cm^{-1}), which are lower than the B–H bending and stretching modes of $(BH_4)^-$ or N–H bending and stretching modes of NH_3. The calculated phonon density of states of the other compounds was not shown here.

Now we calculate the reaction enthalpy and reaction Gibbs free energy of the overall Reactions (2) and (3) as a function of temperature. The vibration contributions were obtained from the phonon densities of states of all solids involved in the reactions. The calculated zero point energies of all the compounds in the

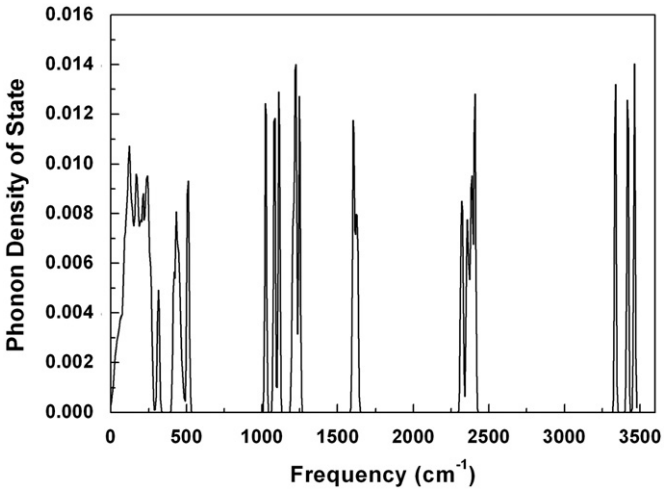

Fig. 6. Calculated total phonon density of states of the $Ca(BH_4)_2 \cdot 2NH_3$.

two reactions are listed in Table 2. The H_2 gas is modeled using the thermodynamic data given by Hemmes et al. [33]. For NH_3 gas, the thermodynamics data in CRC Handbook of Chemistry and Physics (version 2010) was used. The calculated reaction enthalpy and reaction Gibbs free energy for different temperatures of the two reactions are shown in Fig. 7.

At 0 K, the reaction enthalpy is 61.8 kJ/(mol NH_3) for Reaction (2) and 16.9 kJ/(mol H_2) for Reaction (3). When considering the zero point energy (the zero point rotational energy of the hydrogen molecules, 0.011 eV (1.06 kJ/mol), is also included), the enthalpy changes to 12.25 kJ/(mol NH_3) for Reaction (2) and −9.58 kJ/(mol H_2) for Reaction (3). This indicates that Reaction (2) is endothermic and Reaction (3) is exothermic. This is consistent with experimental results. The calculated value of Reaction (3) is also comparable to the experimental value, 13.2 kJ/(mol H_2). For Reaction (2), the reaction enthalpy increases with temperature first and then decreases. For Reaction (3), the temperature effect is small; the reaction enthalpy only changes from −9.85 kJ/(mol H_2) at 0 K to −4.46 kJ/(mol H_2) at 700 K. Next the reaction Gibbs free energy of the two reactions was discussed.

Table 2
Calculated zero point energies of all the compounds in the two reactions. The units are in kJ/mol per formula unit.

$Ca(BH_4)_2 \cdot 2NH_3$	$Ca(BH_4)_2$	$Ca_3(BN_2)_2$	BN	H_2	NH_3
393.5	119.0	54.9	29.3	25.9[a]	87.7[a]

[a] Data in Adv. Mater. 2007, 19, 3233–3239.

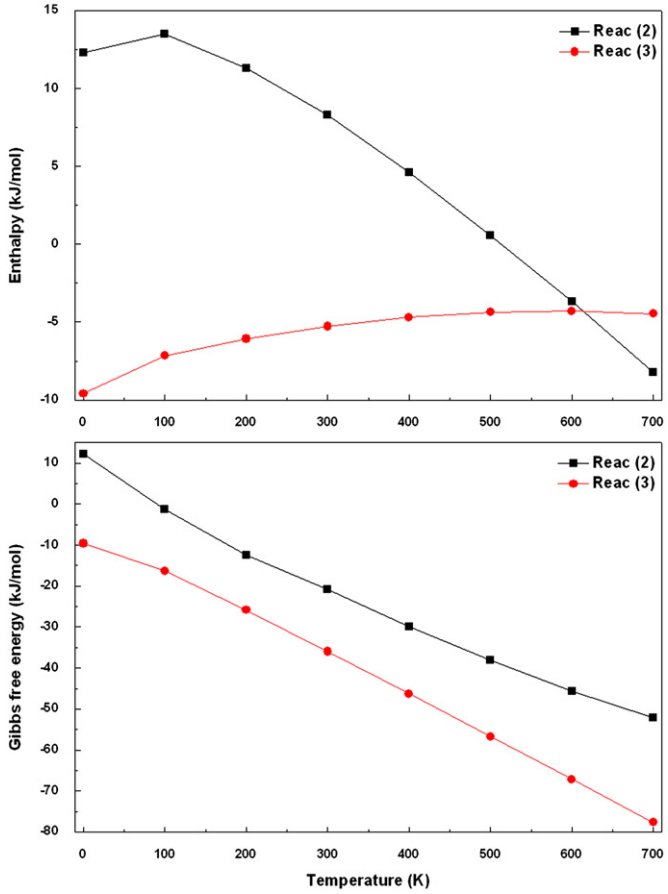

Fig. 7. Calculated reaction enthalpy and reaction Gibbs free energy for overall Reactions (2) and (3) at different temperatures.

From this plot we can see that the reaction Gibbs free energies of both Reactions (2) and (3) decreases with increasing temperature. For Reaction (2), the Gibbs energy changes to zero at about 100 K, indicating that the reaction takes place at this temperature. However the release of NH_3 was observed in experiment at relatively high temperatures above 100 °C. This might suggest that the experimentally observed high temperature for NH_3 release may be a consequence of a higher kinetics barrier. For Reaction (3), the Gibbs energy is always negative which means the reaction should happen at any temperature. In practice, H_2 can be measured only at a high temperature, above 190 °C, and then rapid H_2 release can be obtained above 260 °C [11]. This indicates that the reaction barrier of Reaction (3) is very high. In experiment, the melting of $Ca(BH_4)_2 \cdot 2NH_3$ was also observed at around 230 °C. So the rapid H_2 release occurs from the liquid phase. Combining the experimental and the calculated results, we can propose the following reaction mechanism. For Reaction (2), the mechanism may be simple: the NH_3 diffusion in the solid phase increases with increasing temperature. Hence the gas increases with temperature, as observed experimentally by gradually increased weight loss without an evident decomposition temperature. The calculated energy barrier for NH_3 diffusion along the direction parallel to *y*-axis (see Fig. 8 for detail) is about 1.74 eV. So the mechanism of Reaction (2) may be done to a diffusion mechanism, the NH_3 release rate is limited by its diffusion in the solid. For Reaction (3), the mechanism should be very complex because the solid to liquid phase transition of the reactant occurred in experiment. Here two possible mechanisms were considered, one is that NH_3 diffuses in the solid and reacts with the $(BH_4)^-$ group to produce H_2, then H_2 diffuses from the inner to surface region; the other is that the nearest H^+ in the $(BH_4)^-$ group and H^- in the NH_3 group react to produce H_2, then H_2 diffuses from the inner to surface region. We think the second mechanism may be more impossible in the solid because of the following reason. We calculated the energy cost by simply removing one hydrogen atom or one NH_3 molecule from the unit cell. The energy needed is ~2.0 eV for H in $(BH_4)^-$ group, ~2.9 eV for H in NH_3 group and ~0.91 eV for NH_3, respectively. This result indicates that NH_3 is easier to be removed. So the first mechanism is more reasonable. In this mechanism, the observed H_2 release velocity is effected by many factors, for example, the diffusion velocity of NH_3, the probability of NH_3 reacting with $(BH_4)^-$, the diffusion velocity of H_2. So the releasing velocity of H_2 observed in the experiment is slow at solid phase. When the reaction was

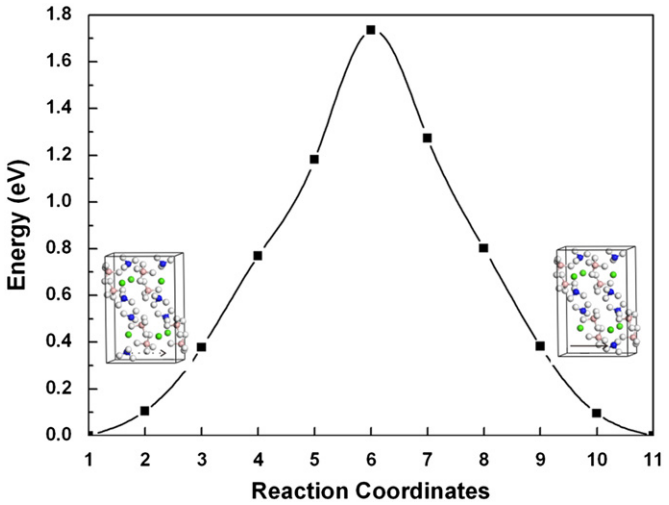

Fig. 8. Calculated energy barrier for NH_3 diffusion along the direction parallel to *y*-axis. The energy of the start position is set at zero.

happened in the liquid phase, the mechanism may change: the compound has large rotational freedom. The distance between H^+ and H^- can be much closer. The second mechanism seems to be more reasonable, because in this mechanism H_2 was produced in one step, the release velocity may be very quick.

4. Conclusion

Theoretical study of newly developed hydrogen storage material $Ca(BH_4)_2 \cdot 2NH_3$ has been carried out to understand its structure and nature of bonding and decomposition. Bond length analyses showed the shortest distance between H^+ and H^- is longer than that in NH_3BH_3. This indicated that the dehydrogenation temperature of $Ca(BH_4)_2 \cdot 2NH_3$ may be higher than NH_3BH_3 if the H_2 is produced directly by the interaction between the nearest H^+ and H^-. Electronic density of states and electron localization function analyses indicated the covalent nature of the N–H bond and the B–H bonds, and the weak ionic bonding between Ca and B or Ca and N. The calculated enthalpy is positive for Reaction (2) and negative for Reaction (3), which indicates the endothermic reaction for NH_3 release and the exothermic reaction for H_2 release. The negative enthalpy of Reaction (3) also means the irreversibility of H_2 release. The findings are consistent with experimental results in the literature. The calculated reaction enthalpy of Reaction (3) is also comparable to experimental value. The possible reaction mechanism of Reactions (2) and (3) was discussed. Our results show that the mechanism of Reaction (3) in solid phase and liquid phase may be different.

Acknowledgment

This work was supported by National Science Foundation of China (Grant nos. 10974182 and 10874154).

References

[1] L. Schlapbach, A. Zuttel, Nature 414 (2001) 353.
[2] R.A. Zidan, S. Takara, A.G. Hee, C.M. Jensen, J. Alloys Compd. 119 (1999) 1.
[3] K.J. Gross, S. Guthrie, S. Takara., G. Thomas, J. Alloys Compd. 297 (2000) 270.
[4] P. Chen, Z. Xiong, J. Luo, J. Lin, L. Tan, Nature (London) 420 (2002) 302.
[5] H.Y. Leng, T. Ichikawa, S. Hino, N. Hanada, S. Isobe, H. Fujii, J. Phys. Chem. B 108 (2004) 8763.
[6] K. Miwa, N. Ohba, S.I. Towata, Y. Nakamori, S.I. Orimo, Phys. Rev. B 69 (2004) 245120.
[7] Y. Nakamori, K. Miwa, A. Ninomiya, H. Li, N. Ohba, S. Towata, A. Zuttel, S. Orimo, Phys. Rev. B 74 (2006) 045126.
[8] N. Ohba, K. Miwa, M. Aoki, T. Noritake, S.I. Towata, Y. Nakamori, S.I. Orimo, A. Zuttel, Phys. Rev. B 74 (2006) 075110.
[9] K. Miwa, M. Aoki, T. Noritake, N. Ohba, Y. Nakamori, S.I. Towata, A. Zuttel, S.I. Orimo, Phys. Rev. B 74 (2006) 155122.
[10] J.H. Kim, S.A. Jin, J.H. Shim, Y.W. Cho, J. Alloys Compd. 461 (2008) L20.
[11] H.L. Chu, G.T. Wu, Z.T. Xiong, J.P. Guo, T. He, P. Chen, Chem. Mater. 22 (2010) 6021.
[12] O. Kravchenko, S. Kravchenko, Zh. Obshch. Khim. 59 (1989) 1935.
[13] W. Kohn, L. Sham, J. Phys. Rev. 140 (1965) A1133.
[14] P.E. Blöchl, Phys. Rev. B 50 (1994) 17953.
[15] G. Kress, D. Joubert, Phys. Rev. B 59 (1999) 1758.
[16] J.P. Perdew, Y. Wang, Phys. Rev. B 45 (1992) 13244.
[17] G. Kresse, J. Hafner, Phys. Rev. B 47 (1993) 558.
[18] G. Kresse, J. Furthmuller, Phys. Rev. B 54 (1996) 11169.
[19] G. Kresse, J. Furthmuller, Comput. Mater. Sci. 6 (1996) 15.
[20] J.P. Perdew, K. Burke, M. Ernzehof, Phys. Rev. Lett. 77 (1996) 3865.
[21] H.J. Monkhorst, J.D. Pack, Phys. Rev. B 13 (1976) 5188.
[22] A.D. Becke, K.E. Edgecombe, J. Chem. Phys. 92 (1990) 5397.
[23] P.E. Blöchl, O. Jepsen, O.K. Andersen, Phys. Rev. B 49 (1994) 16223.
[24] A. Togo, 〈http://fropho.sourceforge.net〉.
[25] J. Senker, M. Muller, W. Press, P. Muller, H.M. Mayer, R.M. Ibberson, J. Phys. Chem. B 102 (1998) 931.
[26] T. Sichla, H. Jacobs, Z. Anorg. Allg. Chem. 622 (1996) 2079.
[27] F. Buchter, J. Phys. Chem. B 112 (2008) 8042.
[28] Y. Filinchuk, E. R€onnebro, D. Chandra, Acta Mater. 57 (2009) 732.
[29] M.E. Bowden, G.J. Gainsford, W.T. Robinson, Aust. J. Chem. 60 (2007) 149.
[30] P. Choudhury, V.R. Bhethanabotla, E. Stefanakos, Phys. Rev. B 77 (2008) 134302.
[31] G. Henkelamn, A. Arnaldsson, H. Jonsson, Comput. Mater. Sci. 36 (2006) 354–360.
[32] E. Jeon, Y. Cho, J. Alloys Compd. 422 (2006) 273.
[33] H. Hemmes, A. Driessen, R. Griessen, J. Phys. C 19 (1986) 3571.